Available online at www.sciencedirect.com
ScienceDirect
Trans. Nonferrous Met. Soc. China 20(2010) 607−613
Transactions of Nonferrous Metals Society of China
www.tnmsc.cn

Structures and electrochemical performances of $La_{0.75-x}Zr_xMg_{0.25}Ni_{3.2}Co_{0.2}Al_{0.1}$ (x=0−0.2) electrode alloys prepared by melt spinning

ZHANG Yang-huan(张羊换)[1, 2], ZHAO Dong-liang(赵栋梁)[1], SHI Yan-chun(师颜春)[1, 2],
QI Yan(祁 焱)[1], GUO Shi-hai(郭世海)[1], WANG Xin-lin(王新林)[1]

1. Department of Functional Material Research, Central Iron and Steel Research Institute, Beijing 100081, China;
2. School of Material, Inner Mongolia University of Science and Technology, Baotou 014010, China

Received 6 March 2009; accepted 30 June 2009

Abstract: The La-Mg-Ni system A_2B_7-type electrode alloys with nominal composition $La_{0.75-x}Zr_xMg_{0.25}Ni_{3.2}Co_{0.2}Al_{0.1}$ (x=0, 0.05, 0.1, 0.15, 0.2) were prepared by casting and melt-spinning. The influences of melt spinning on the electrochemical performances as well as the structures of the alloys were investigated. The results obtained by XRD, SEM and TEM show that the as-cast and spun alloys have a multiphase structure, consisting of two main phases (La, Mg)Ni_3 and $LaNi_5$ as well as a residual phase $LaNi_2$. The melt spinning leads to an obvious increase of the $LaNi_5$ phase and a decrease of the (La, Mg)Ni_3 phase in the alloys. The results of the electrochemical measurement indicate that the discharge capacity of the alloys ($x\leqslant0.1$) first increases and then decreases with the increase of spinning rate, whereas for $x>0.1$, the discharge capacity of the alloys monotonously falls. The melt spinning slightly impairs the activation capability of the alloys, but it significantly enhances the cycle stability of the alloys.
Key words: A_2B_7-type electrode alloy; La-Mg-Ni alloy; Ni-MH battery; melt-spinning; electrochemical performance

1 Introduction

Recently, the European Community and major developed countries world-widely banned the use of cadmium in batteries, which effectively prevented continuing use of Ni-Cd power battery. This provides a golden opportunity for the development of the Ni-MH battery. However, none of the currently commercialized electrode alloys as negative electrode material of Ni-MH battery, including AB_5 and AB_2-types, can meet the demand of the power battery owing to the limitation of their properties. The discharge capacity of the AB_5-type electrode alloy is comparatively low and the activation capability of the AB_2-type Laves phase electrode alloys is very poor. Therefore, it is one of the serious challenges for researchers in this area to find new electrode alloys with higher capacity and longer cycle life.

Recently, some of the new series of RE-Mg-Ni-based (where RE is a rare earth or Y, Ca) AB_3-type alloys were considered to be most promising candidates owing to their higher discharge capacities (360−410 mA·h/g) and low production costs. KADIR et al[1−4] revealed that this kind of alloys hold $PuNi_3$-type rhombohedral structure. KOHNO et al[5] found that the $La_5Mg_2Ni_{23}$-type electrode alloy $La_{0.7}Mg_{0.3}Ni_{2.8}Co_{0.5}$ has a capacity of 410 mA·h/g and good cycle stability during 30 charge-discharge cycles. PAN et al[6] investigated the structures and electrochemical characteristics of the $La_{0.7}Mg_{0.3}(Ni_{0.85}Co_{0.15})_x$ (x=3.15−3.80) alloy system and obtained a maximum discharge capacity of 398.4 mA·h/g. however, the cycle stability of the alloy needs to be improved further. LI et al[7] researched the influence of the substitution of Ce, Pr and Nd for La on the structure and electrochemical behaviours of the La-Mg-Ni based alloys, and the results showed that the substitution led to a decrease of the discharge capacity and obvious improvement of the cycle stability of the alloys. BANCZEK et al [8] reported that the alloy without Pr and the one with total La substitution showed the highest corrosion resistance among the $La_{0.7-x}Pr_xMg_{0.3}Al_{0.3}Mn_{0.4}$-$Co_{0.5}Ni_{3.8}$ (x=0, 0.1, 0.3, 0.5, and 0.7) alloys.

Foundation item: Project(2007AA03Z227) supported by High-tech Research and Development Program of China; Projects(50871050, 50701011) supported by the National Natural Science Foundation of China; Project(200711020703) supported by the Natural Science Foundation of Inner Mongolia, China; Project(NJzy08071) supported by High Education Science Research Project of Inner Mongolia, China
Corresponding author: ZHANG Yang-huan; Tel: +86-10-62187570; E-mail: zyh59@yahoo.com.cn
DOI: 10.1016/S1003-6326(09)60186-2

Although the investigation on the structure and electrochemical properties of the alloys has obtained very important progress, their poor cycle stability has to be further improved for commercial application. It is well known that element substitution is one of the effective methods for improving the overall properties of the hydrogen storage alloys. In addition，the preparation technology is also important for improving the performances of the alloys. It is well known that element Zr is able to absorb hydrogen and promote the formation of an amorphous phase. Therefore, Zr is chosen as the substitution element in order to obtain an amorphous phase in the as-spun alloy. It is expected that the combination of an optimized amount of Zr substitution for La with a proper melt spinning technique may lead to an alloy with high discharge capacity and good cycling stability. For this purpose, the influences of melt spinning on the structures and electrochemical performances of the $La_{0.75-x}Zr_xMg_{0.25}Ni_{3.2}Co_{0.2}Al_{0.1}$ (x=0, 0.05, 0.1, 0.15, 0.2) electrode alloys are systematically investigated.

2 Experimental

2.1 Preparation of alloy

The nominal composition of the experimental alloys was $La_{0.75-x}Zr_xMg_{0.25}Ni_{3.2}Co_{0.2}Al_{0.1}$($x$=0, 0.05, 0.1, 0.15, 0.2). For convenience, the alloys were denoted with Zr content as Zr_0, Zr_1, Zr_2, Zr_3 and Zr_4, respectively. The alloy ingots were prepared using a vacuum induction furnace in a helium atmosphere at a pressure of 0.04 MPa. Part of the as-cast alloys were re-melted and spun by melt-spinning with a rotating copper roller. The spinning rate was approximately expressed by the linear velocity of the copper roller because it is difficult to measure a real spinning rate, i.e. cooling rate of the sample during spinning. The spinning rates used in the experiment were 5, 10, 15 and 20 m/s, respectively.

2.2 Analysis of microstructure

The cast ingot and spun ribbons were mechanically crushed and ground into powder of about 40 μm for X-ray diffraction (XRD) analysis. The phase structures and compositions of the alloys were determined by X-ray diffractometer of D/max/2400. The diffraction, with the experimental parameters of 160 mA, 40 kV and 10 (°)/min respectively, was performed with Cu $K_{\alpha 1}$ radiation filtered by graphite. The morphologies of the as-cast alloys were examined by SEM (Philips QUANTA 400). Thin film samples of the as-spun alloys were prepared by ion etching for observing the grain morphology with TEM (JEM-2100F), and for determining crystalline state of the samples with selected area electron diffraction (SAED).

2.3 Measurement of electrochemical performance

Round electrode pellets of 15 mm in diameter were prepared by cold pressing a mixture of the alloy powder and carbonyl nickel powder in a mass ratio of 1:4 with a pressure of 35 MPa. After being dried for 4 h, the electrode pellets were immersed in a 6 mol/L KOH solution for 24 h in order to wet fully the electrodes before the electrochemical measurement.

A tri-electrode open cell, consisting of a metal hydride electrode, a $NiOOH/Ni(OH)_2$ counter electrode and a Hg/HgO reference electrode, was used for testing the electrochemical performance of the experimental electrodes. The electrolyte was a 6 mol/L KOH solution. The voltage between the negative electrode and the reference electrode was defined as the discharge voltage. In every cycle, the alloy electrode was firstly charged with a constant current density. After resting for 15 min, it was discharged at a same current density to cut-off voltage of −0.500 V. The environmental temperature of the measurement was kept at 30 ℃.

3 Results and discussion

3.1 Influence of melt spinning on structure

The XRD patterns of the Zr_0 and Zr_4 alloys are shown in Fig.1, revealing that the as-cast and spun alloys hold a multiphase structure, consisting of two major phases (La, Mg)Ni_3 and $LaNi_5$ as well as a residual phase $LaNi_2$. It can be seen in Fig.1 that the melt spinning causes the major diffraction peaks of the alloys obviously broadened. Listed in Table 1 are the full width at half maximum (FWHM) values of the main diffraction peaks of the Zr_0 and Zr_4 alloys, which were calculated by software of Jade 6.0. It can be derived from Table 1 that melt spinning produces broader diffuse peaks, indicating the refinement of the average grain size and stored stress in the grains. The lattice parameters and the amount of the $LaNi_5$ and the (La, Mg)Ni_3 major phases in the Zr_0 and Zr_4 alloys calculated from the XRD data are listed in Table 2. It can be derived from Table 2 that the melt

Table 1 FWHM values of major diffraction peaks of Zr_0 and Zr_4 alloys

Spinning rate/(m·s^{-1})	FWHM value			
	2θ (42.3°)		2θ (35.4°)	
	Zr_0	Zr_4	Zr_0	Zr_4
0	0.167	0.374	0.182	0.256
5	0.181	0.405	0.221	0.309
10	0.244	0.472	0.231	0.373
15	0.265	0.502	0.239	0.405
20	0.322	0.620	0.319	0.503

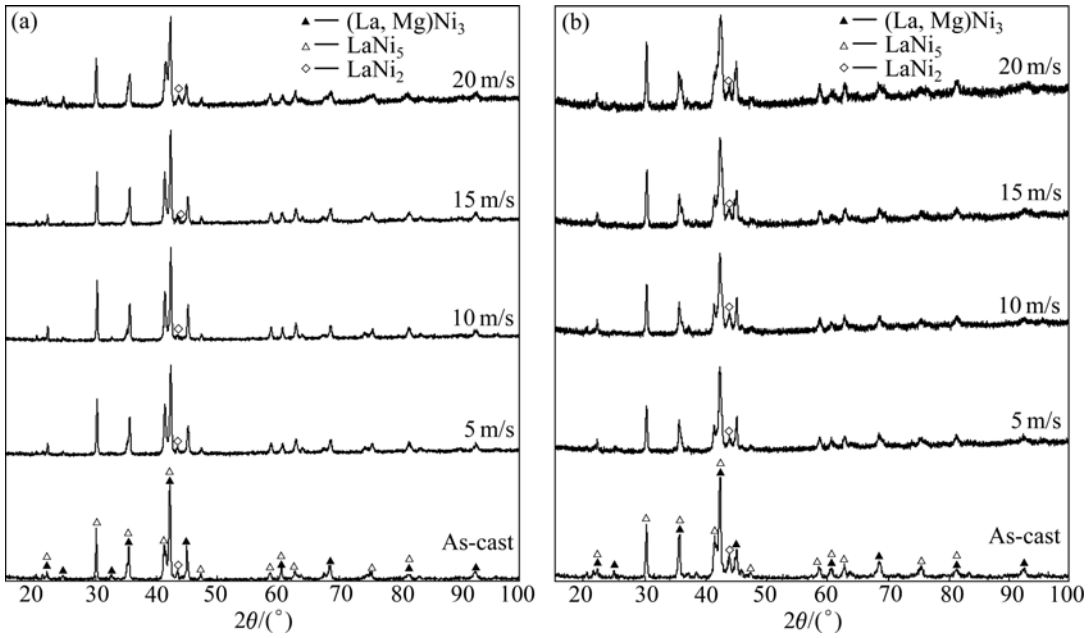

Fig.1 XRD patterns of the as-cast alloy and spun alloys at different spinning rate: (a) Zr_0 alloy; (b) Zr_4 alloy

Table 2 Lattice constants and amount of $LaNi_5$ and $(La, Mg)Ni_3$ major phases

Alloy	Spinning rate/(m·s^{-1})	Major phase	Lattice constant/nm		Cell volume/nm^3	Phase content/%
			a	*c*		
Zr_0	0	$(La, Mg)Ni_3$	0.520 4	2.440 1	0.572 2	74.35
		$LaNi_5$	0.519 7	0.417 8	0.097 7	24.07
	5	$(La, Mg)Ni_3$	0.520 1	2.440 3	0.571 7	73.57
		$LaNi_5$	0.519 4	0.417 8	0.097 6	25.02
	10	$(La, Mg)Ni_3$	0.519 9	2.440 6	0.571 2	72.31
		$LaNi_5$	0.519 2	0.418 0	0.097 6	25.24
	15	$(La, Mg)Ni_3$	0.519 7	2.440 8	0.570 9	72.02
		$LaNi_5$	0.519 0	0.418 1	0.097 5	25.83
	20	$(La, Mg)Ni_3$	0.519 7	2.440 9	0.570 9	71.52
		$LaNi_5$	0.518 9	0.418 3	0.097 5	26.27
Zr_0	0	$(La, Mg)Ni_3$	0.496 6	2.416 7	0.516 1	58.33
		$LaNi_5$	0.493 6	0.401 8	0.084 8	39.24
	5	$(La, Mg)Ni_3$	0.496 4	2.417 1	0.515 8	58.18
		$LaNi_5$	0.493 3	0.402 0	0.084 7	39.24
	10	$(La, Mg)Ni_3$	0.496 3	2.417 4	0.515 6	58.02
		$LaNi_5$	0.493 3	0.402 1	0.084 7	39.32
	15	$(La, Mg)Ni_3$	0.496 1	2.417 8	0.515 3	57.85
		$LaNi_5$	0.493 2	0.402 1	0.084 7	39.35
	20	$(La, Mg)Ni_3$	0.496 1	2.418 0	0.515 3	57.27
		$LaNi_5$	0.493 2	0.402 2	0.084 7	39.49

spinning leads to *c* axis increased and the *a* axis and cell volume of the $LaNi_5$ and the $(La, Mg)Ni_3$ main phases slightly decreased, which results in the increase of the amount of $LaNi_5$ phase and the decrease of the $(La, Mg)Ni_3$ phase. It is noteworthy that, for a fixed spinning rate, the amount of the $LaNi_5$ phase in the Zr_0 alloys is less than that in the Zr_4 alloy, whereas the amount of the $(La, M)Ni_3$ phase in the Zr_0 alloys is more than that in the Zr_4 alloy, suggesting that the substitution of Zr for La leads to the increase of the $LaNi_5$ phase and the decrease

of the (La, Mg)Ni_3 phase.

The SEM images and EDS spectra of the as-cast alloys are shown in Fig.2. The results indicate that both the experimental alloys are of multiphase structure, containing the (La, Mg)Ni_3 (denoted as A) and the $LaNi_5$ (denoted as B) phases, which is in agreement with the results of XRD analysis. Because the amount of the $LaNi_2$ phase is small and it attaches to the (La, Mg)Ni_3 phase or the $LaNi_5$ phase in the process of growing, it is difficult to observe the morphology of the $LaNi_2$ phase. It can be seen in Fig.2 that the substitution of Zr for La leads to the grains of the as-cast alloys significantly refined.

The morphologies and the crystalline states of the as-spun alloys were examined by TEM as shown in Fig.3. It can be seen that the as-spun (10 m/s) Zr_0 alloy exhibits a nano-crystalline and microcrystalline structure. The electron diffraction pattern of the as-spun (10 m/s) Zr_4 alloy shows broad and dull halo, indicating the formation of an amorphous like structure. This seems to be conflicting with the result in Fig.1 which does not show an appearance of amorphous phase. A probable reason is that the amorphous like phase forms at some selective location in the as-spun alloy and its amount is very small, so the XRD patterns do not clearly exhibit the presence of an amorphous phase. Based on the result in Fig.3, it can be concluded that the substitution of Zr for La favors the formation of an amorphous phase in the as-spun alloy.

3.2 Influence of melt spinning on electrochemical performance

3.2.1 Activation capability and discharge capacity

The activation capability was characterized by the number of charging-discharging cycles required for attaining the greatest discharge capacity at a constant current density of 100 mA/g. The fewer the number of charging-discharging cycle, the better the activation performance. The evolution of the discharge capacities of the as-cast and spun alloys with cycle number is plotted in Fig.4, which indicates that all the as-cast and spun alloys possess excellent activation performances, attaining their maximum discharge capacities after 1 to 2 charging-discharging cycles. The melt spinning slightly impairs the activation capability of the as-cast alloys.

Generally, the activation capability of the hydrogen storage alloy is directly relevant to the change of the internal energy (involving the surface energy which originates from oxidation film formed on the surface of the electrode alloy and the strain energy which is produced by hydrogen atom entering the interstitial of the tetrahedron or octahedron of the alloy lattice) of the hydride system before and after absorbing hydrogen. The larger the additive internal energy, the poorer the activation performance of the alloy[9]. Two explanations may be offered as the reason why the melt spinning impairs the activation performances of the as-cast and spun alloys. Firstly, the melt spinning reduces the cell volumes of the alloys, increasing the ratios of expansion/

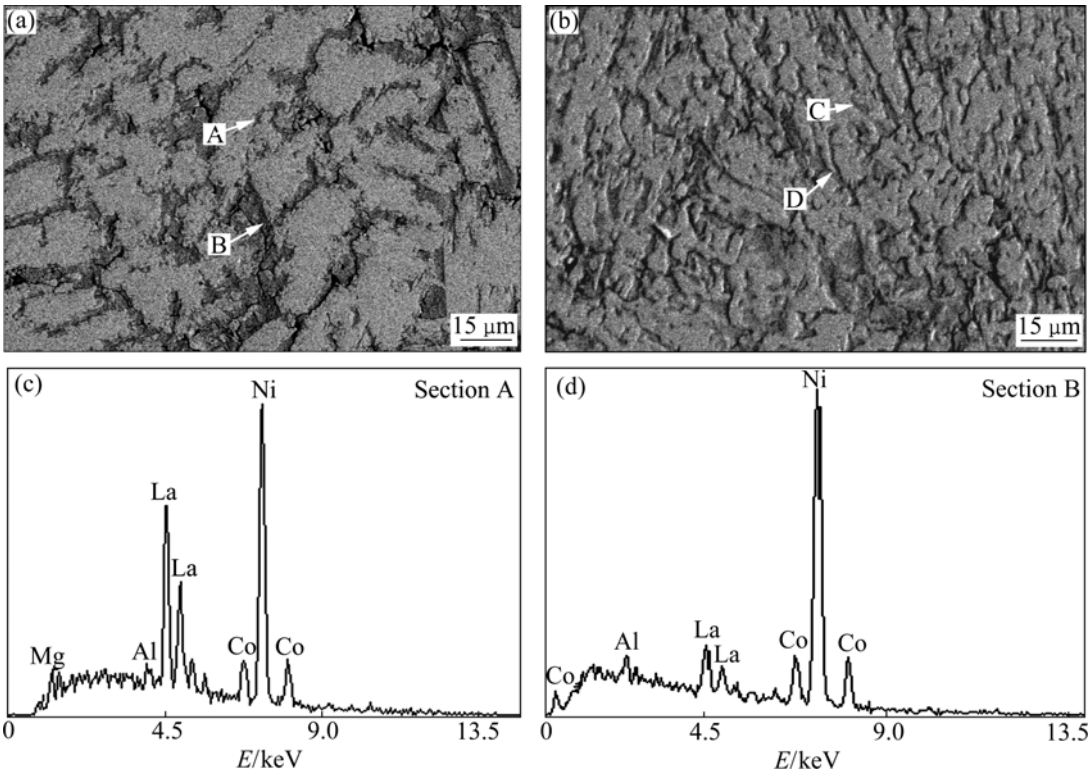

Fig.2 SEM images of as-cast alloys: (a) Zr_0 alloy; (b) Zr_4 alloy; (c, d) EDS spectra of Zr_0 alloy

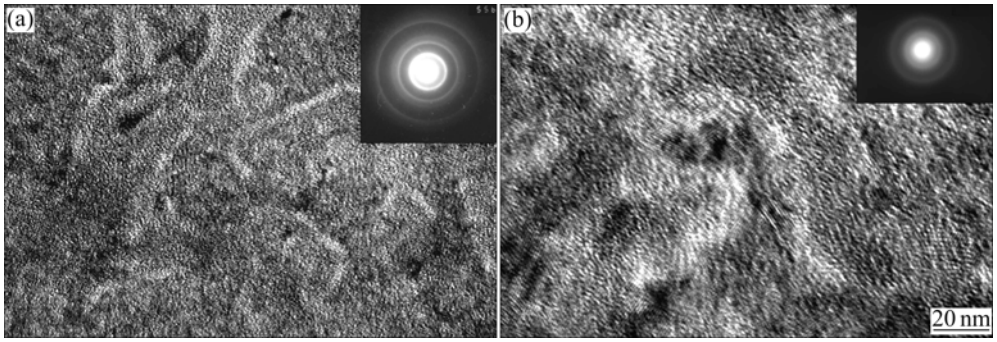

Fig.3 TEM morphologies and SAED patterns of as-spun alloys (10 m/s): (a) Zr_0 alloy; (b) Zr_4 alloy

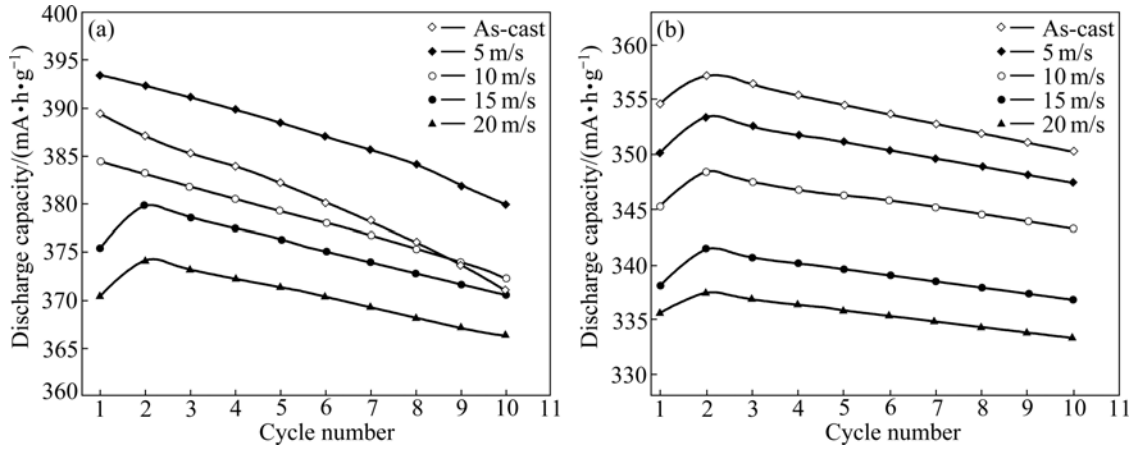

Fig.4 Activation capability of as-cast and spun alloys: (a) Zr_0 alloy, (b) Zr_4 alloy

contraction of the alloys in the process of the hydrogen absorption/desorption, which means increasing the strain energy. Secondly, the melt spinning leads to the increase of lattice stress and the decrease of the electrocatalytic activity of the alloy electrodes.

The maximum discharge capacity of the alloys as a function of the spinning rate is shown in Fig.5, at a charge-discharge current density of 100 mA/g. It can be clearly seen in Fig.5 that with the increase of the spinning rate, the discharge capacities of the alloys ($x \leqslant 0.1$) first increase and then decrease, but the discharge capacities of the alloys ($x > 0.1$) monotonously fall. When the spinning rate rises from 0 (as-cast was defined as spinning rate of 0 m/s) to 20 m/s, the discharge capacity increases from 371.6 (at 0 m/s) to 374.7 mA·h/g (at 5 m/s), after that drops to 357.6 mA·h/g (at 20 m/s) for the Zr_2 alloy, and it monotonously declines from 357.2 to 337.4 mA·h/g for the Zr_4 alloys. The above-mentioned result is relevant to the change of the phase contents and structure of the alloys caused by the melt spinning.

The amount of the $LaNi_5$ phase in the alloy increases with increasing spinning rate, which is disadvantageous to the discharge capacity of the alloy due to the fact that the discharge capacity of the $LaNi_5$ phase is lower than that of the (La, Mg)Ni_3 phase[10−11]. However, it is noteworthy that the $LaNi_5$ phase works not only as a hydrogen reservoir but also as a catalyst to activate the (La,Mg)Ni_3 phase to absorb/desorb reversibly hydrogen in the alkaline electrolyte[12]. It is the above contrary effects that result in an optimum spinning rate for the discharge capacities of the alloys. For Zr content $x > 0.1$, the discharge capacity of the alloy monotonously declines with increasing spinning rate. It

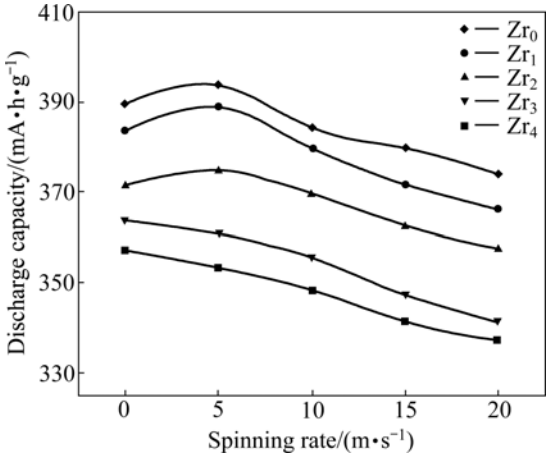

Fig.5 Evolution of discharge capacities of alloys with spinning rate

is attributed to two factors, i.e. the formation of an amorphous phase and the increase of the $LaNi_5$ phase caused by melt spinning, which are disadvantageous for the discharge capacity of the alloy because the capacity of the amorphous phase is half as large as that of the crystalline alloy[13]. Therefore, it is self-evident that the discharge capacity of the alloy monotonously declines with increasing spinning rate.

3.2.2 Cycle stability

The capacity retaining rate (S_n) is introduced for accurately evaluating the cycle stability of the alloy. It is defined as $S_n=(C_n/C_{max})\times100\%$, where C_{max} is the maximum discharge capacity, and C_n is the discharge capacity of the nth cycle at a current density of 600 mA/g. The capacity retaining rate (S_{100}) of the alloys as a function of the spinning rate is illustrated in Fig.6. It can be derived from Fig.6 that the capacity retaining rate (S_{100}) of the alloys rises with the increase of the spinning rate, meaning that the melt spinning improves the cycle stability of the alloys. When the spinning rate increases from 0 to 20 m/s, the capacity retaining rate (S_{100}) increases from 65.32% to 73.97% for Zr_0 alloy, and from 76.69% to 85.18% for Zr_4 alloy.

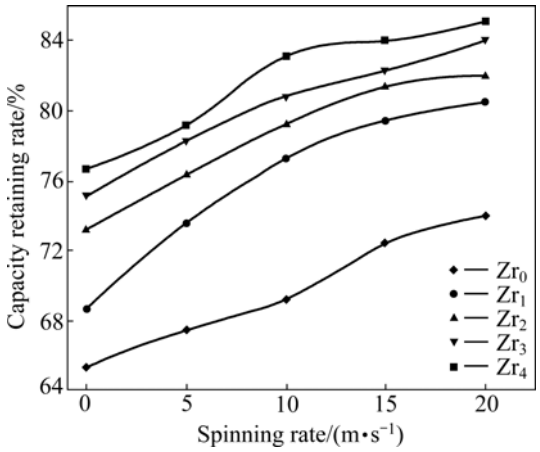

Fig.6 Capacity retaining rate (S_{100}) of alloys as function of spinning rate

In order to clearly show the process of capacity degradation of the alloy electrode, the evolution of capacity retaining rates of the Zr_0 and Zr_4 alloys with the cycle number is shown in Fig.7. A rough tendency can be seen in Fig.7 that the decay rates of the discharge capacities of the Zr_0 and Zr_4 alloys with cycle number obviously decrease with rising spinning rate, suggesting that the melt spinning enhances the cycle stability of the alloys.

The electrode failure is characterized by the decay of the discharge capacity and the drop of the discharge voltage. It was confirmed by Refs.[14−15] that the fundamental reasons for the capacity decay of the electrode alloy are the pulverization and the oxidation of

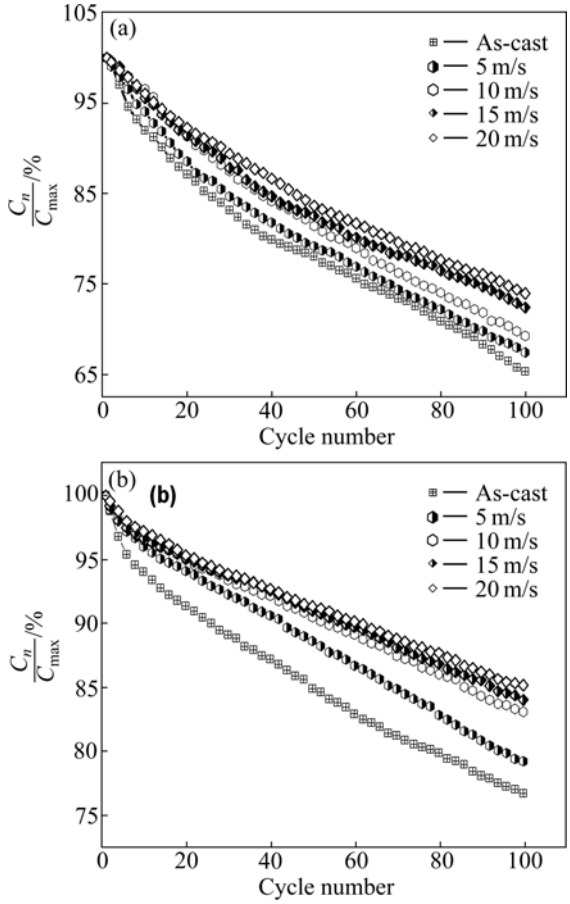

Fig.7 Evolution of capacity retaining rates of alloys with cycle number: (a) Zr_0 alloy; (b) Zr_4 alloy

the alloy during charging-discharging cycle. The lattice stress and the expansion of the cell volume, which are inevitable when hydrogen atoms enter into the interstitials of the lattice, are the real driving force that leads to the pulverization of the alloy. The positive impact of the melt spinning on the cycle stability of the alloy is primarily ascribed to the significant refinement of the grains and the formation of an amorphous phase. The anti-pulverization capability of the alloy basically depends on its grain size. An amorphous phase improves not only anti-pulverization ability but also anti-corrosion and anti-oxidation abilities of the alloy electrode in a corrosive electrolyte [16−18]. Therefore, it is understandable that the cycle stability of the alloy increases with rising spinning rate.

4 Conclusions

1) The melt spinning does not change the phase compositions of the $La_{0.75-x}Zr_xMg_{0.25}Ni_{3.2}Co_{0.2}Al_{0.1}$ (x=0, 0.05, 0.1, 0.15, 0.2) alloys, but it causes the amount of $LaNi_5$ phase to increase and the amount of (La, Mg)Ni_3 phase to decrease in the alloys. In addition, the melt spinning leads to the grains of the alloy significantly

refining, and it obviously reduces the lattice constants and cell volumes of the alloys.

2) The melt spinning exerts an obviously influence on the electrochemical performances of the alloys. The discharge capacities of the alloys ($x \leqslant 0.1$) reach the maximum values at a special spinning rate. The melt spinning slightly impairs the activation capability of the alloys, but it significantly improves the cycle stability of the alloys, which is attributed to the refinement of the grains of the alloys and the formation of an amorphous produced by the melt spinning.

References

[1] KADIR K, SAKAI T, UEHARA I. Synthesis and structure determination of a new series of hydrogen storage alloys: RMg_2Ni_9 (R=La, Ce, Pr, Nd, Sm and Gd) built from $MgNi_2$ Laves-type layers alternating with AB_5 layers [J]. J Alloys Comp, 1997, 257: 115−121.

[2] KADIR K, KURIYAMA N, SAKAI T, UEHARA I, ERIKSSON L. Structural investigation and hydrogen capacity of $CaMg_2Ni_9$: A new phase in the AB_2C_9 system isostructural with $LaMg_2Ni_9$ [J]. J Alloys Comp, 1999, 284: 145−154.

[3] KADIR K, SAKAI T, UEHARA I. Structural investigation and hydrogen capacity of YMg_2Ni_9 and $(Y_{0.5}Ca_{0.5})(MgCa)Ni_9$: New phases in the AB_2C_9 system isostructural with $LaMg_2Ni_9$ [J]. J Alloys Comp, 1999, 287: 264−270.

[4] KADIR K, SAKAI T, UEHARA I. Structural investigation and hydrogen storage capacity of $LaMg_2Ni_9$ and $(La_{0.65}Ca_{0.35})$-$(Mg_{1.32}Ca_{0.68})Ni_9$ of the AB_2C_9 type structure [J]. J Alloys Comp, 2000, 302: 112−117.

[5] KOHNO T, YOSHIDA H, KAWASHIMA F, INABA T, SAKAI I, YAMAMOTO M, KANDA M. Hydrogen storage properties of new ternary system alloys: La_2MgNi_9, $La_5Mg_2Ni_{23}$, La_3MgNi_{14} [J]. J Alloys Comp, 2000, 311: L5−L7.

[6] PAN H G, LIU Y F, GAO M X, ZHU Y F, LEI Y Q, WANG Q D. An investigation on the structural and electrochemical properties of $La_{0.7}Mg_{0.3}(Ni_{0.85}Co_{0.15})_x$ (x=3.15−3.80) hydrogen storage electrode alloys [J]. J Alloys Comp, 2003, 351: 228−234.

[7] LI Y, HAN D, HAN S M, ZHU X L, HU L, ZHANG Z, LIUY W. Effect of rare earth elements on electrochemical properties of La-Mg-Ni-based hydrogen storage alloys [J]. Int J Hydrogen Energy, 2009, 34: 1399−1404.

[8] BANCZEK E P, ZARPELON L M C, FARIA R N, COSTA I. Corrosion resistance and microstructure characterization of rare-earth-transition metal-aluminum-magnesium alloys [J]. J Alloys Comp, 2009, 479: 342−347.

[9] WU M S, WU H R, WANG Y Y, WAN C C. Surface treatment for hydrogen storage alloy of nickel/metal hydride battery [J]. J Alloys Comp, 2000, 302: 248−257.

[10] OESTERREICHER H, CLINTON J, BITTNER H. Hydrides of La-Ni compounds [J]. Mater Res Bull, 1976, 11: 1241−1247.

[11] TAKESHITA T, WALLACE W E, CRAIG R S. Rare earth intermetallics as synthetic ammonia catalysts [J]. Inorg Chem, 1974, 13: 2282−2283.

[12] PAN H G, LIU Y F, GAO M X, LEI Y Q, WANG Q D. A study of the structural and electrochemical properties of $La_{0.7}Mg_{0.3}$-$(Ni_{0.85}Co_{0.15})_x$ (x=2.5−5.0) hydrogen storage alloys [J]. J Electrochem Soc, 2003, 150(5): A565−A570.

[13] LI Y, CHENG Y T. Amorphous La-Ni thin film electrodes [J]. J Alloys Comp, 1995, 223: 6−12.

[14] LIU Y F, PAN H G, GAO M X, LEI Y Q, WANG Q D. XRD study on the electrochemical hydriding/dehydriding behavior of the La-Mg-Ni-Co-type hydrogen storage alloys [J]. J Alloys Comp, 2005, 403: 296−304.

[15] CHARTOUNI D, MELI F, ZÜTTEL A, GROSS K, SCHLAPBACH L. The influence of cobalt on the electrochemical cycling stability of $LaNi_5$-based hydride forming alloys [J]. J Alloys Comp, 1996, 241:160−166.

[16] ZHANG Y H, LI B W, REN H P, CAI Y, DONG X P, WANG X L. Investigation on structures and electrochemical performances of the as-cast and quenched $La_{0.7}Mg_{0.3}Co_{0.45}Ni_{2.55-x}Fe_x$ (x=0−0.4) electrode alloys [J]. Int J Hydrogen Energy, 2007, 32: 4627−4634.

[17] ZHANG Y H, CHEN M Y, WANG X L, WANG G Q, LIN Y F, QI Y. Effect of boron additive on the cycle life of low-Co AB_5-type electrode consisting of alloy prepared by cast and rapid quenching [J]. J Power Sources, 2004, 125: 273−279.

[18] ZHANG Y H, ZHAO D L, DONG X P, QI Y, GUO S H, WANG XL. Effects of rapid quenching on structure and electrochemical characteristics of $La_{0.5}Ce_{0.2}Mg_{0.3}Co_{0.4}Ni_{2.6-x}Mn_x$ (x=0−0.4) electrode alloys [J]. Transactions of Nonferrous Metals Society of China, 2009, 19(2): 364−371.

(Edited by FANG Jing-hua)